

ENHANCED OPTICAL, STRUCTURAL AND ANTIBACTERIAL PROPERTIES OF ZnO DOPED TiO₂ COMPOSITES

Mehmet Eymen Sümer^a, Bengü Özüğur Uysal^{b*}

^a *Computational Biology and Genetics, School of Graduate Studies, Kadir Has University, Cibali, Fatih, Istanbul 34083, Turkey*

^b *Faculty of Engineering and Natural Sciences, Kadir Has University, Cibali, Fatih, Istanbul 34083, Turkey*

* *Corresponding author*

Tel: +90 212 533 65 32 / 1345

Fax: +90 212 533 65 15

e-mail(s): bozugur@khas.edu.tr

ABSTRACT

In daily life, bacterial infections are common issues for human health. Thus, researchers are searching for valuable materials to prevent antibacterial infections and environmental pollutants. Thin film is a well-known application for photocatalytic and biological activity. Hence, thin-film formation is an excellent way to overcome these problems due to its nanosize thickness and enhanced monolayer or a multilayered structure. The most common material to produce a thin film is titanium oxide (TiO₂). It has various traits to enhance the activity of thin films, such as structural and optical properties. However, single usage of pure TiO₂ has some limitations over these problems. Therefore, new techniques need to be implemented to overcome these limitations, and it is called doping. Doping is a standard method for manipulating material properties to provide enhanced functionality. Thus, ZnO was selected as a dopant due to its good bandgap energy and high electron activity. Therefore, this research mainly focused on the antibacterial, structural, and optical activity differences of pure TiO₂ and ZnO doped TiO₂. The sol-gel method was used in this research for several different thin film deposition methods due to its easy progression at room temperature, low cost, and homogeneity traits. Antibacterial activity of pure and doped TiO₂ thin films was analyzed by the standard of ISO 22196 protocol against gram-positive “*Staphylococcus aureus*” and gram-negative “*Escherichia coli*”. As a result, XRD and UV-vis spectrophotometer measurements show

that our dopant ZnO efficiently enhances the bandgap energy of pure TiO₂, and the correlation between dispersibility and homogeneity was achieved in the concentration range ZTA-B-R (5-10).

Keywords: ZnO Doped TiO₂, Sol-gel thin films, XRD, UV-vis spectrophotometer, Antibacterial coatings

1. INTRODUCTION

Material science and bioengineering are important majors of human life. Thus, the collaboration of these two majors can be beneficial for biotechnological advancement. In recent years, environmental problems have increased rapidly due to the waste product of many applications¹. Due to the high amount of waste products, many researchers use nanocomposites (NC) as a bypass mechanism for the antibacterial inhibition of waste products. Thin-film application is a well-known method for enhancing the activity of antibacterial inhibition and photocatalytic activation by using nanocomposites. NCs are critical materials for many biological applications^{2 3}. Therefore, finding proper concentration and combination of nanocomposites in the thin-film application is essential for the activity level of the material. However, in some applications, the single nanoparticle may not be efficient, and some material addition is required to enhance the activity level of the material, which is called a dopant. Therefore, dopant materials are generally used to enhance the activity level of the initial material by changing the materials' initial bandgap energy. Thus, the addition and selection of proper dopant material is crucial for a succession of research because not every dopant can synergize with every nanoparticle. Therefore, before starting this research, most of the dopants and their collaboration with nanoparticles were determined. In the selection period, three main criteria arise; the first one is dopant material suitable for this experimental methodology, the second one is dopant's ability to enhance antibacterial effects, and the third one is dopant synergize with an initial nanoparticle. Therefore, before starting any antibacterial experiment with the nanoparticle, these topics need to be checked for further implementation. Primary materials need to be multifunctional. Titanium dioxide (TiO₂) is a transition metal, and it is a valuable material for material science and biomedicine.

Titanium dioxide (TiO_2) has a bright white color, and it has three crystalline phases: anatase, brookite, and rutile. Titanium dioxide (TiO_2) is an excellent semiconductor in terms of bandgap energy, such as anatase 3.20 eV, rutile 3.00 eV, and brookite 3.13 eV⁴⁻⁶. Titanium oxide (TiO_2) is one of the most favorable materials for its multifunctional traits. Titanium oxide (TiO_2) is also a promising material due to its photocatalytic, semi-conductive, high degradation, easy to process, and low-cost traits⁷. In addition, titanium dioxide (TiO_2) has multifunctional traits such as high recombination rate, biodegradability, and photocatalytic activity in higher temperatures⁸. The anatase and brookite phases naturally transform into the rutile phase under high temperatures, and this trait makes the rutile phase the most stable phase⁹. Its morphology highly depends on its phase differences and chemical manipulation, such as dopant addition. Anatase, brookite and rutile are the three main phases of TiO_2 ⁷. All these phases have distinct abilities and provide different advantages due to their different structural and chemical activities. For example, anatase has a tetragonal structure, and brookite has an orthorhombic structure⁹. Moreover, the anatase phase is the initial phase formed in many applications, and then it transforms into brookite and rutile in high temperatures, respectively.

Anatase has the largest bandgap than other phases, and this trait makes anatase more photocatalytic than the others⁷. However, rutile can be more stable in higher temperatures and has the highest refractive index⁸. Transformation of anatase to the rutile phase is irreversible. Brookite is rarely seen compared to anatase and rutile because its production is too hard for lab conditions. However, brookite has the most significant cell volume. That feature makes the brookite phase valuable for biomedical and environmental treatments⁹. TiO_2 is used in various areas such as dye-sensitized solar cells, ion batteries, gas sensors, filters, light sensors, humidity sensors, hydrogen sensors, tissue engineering, biomedical and biodegradable treatments, industrial dyes, textiles, and environmental remediation⁸. However, sometimes using a single material can produce some problems because of materials' limitations but these limitations are overcome by using dopants. Many studies show that mixed phases are more impactful than pure TiO_2 because of their limitations¹⁰. A cross-section of these limitations needs to be handled correctly to get the desired result¹¹.

Therefore, the additional dopants -as mentioned before-need to be selected to synergize with titanium oxide and overcome its limitations. Every dopant has different bandgap

energy, recombination rate, electron mobility, surface structure, and other features. Thus, dopants generally enhance the activity of primary material due to their beneficial effects on structural, morphological, chemical, and physical traits (Khlyustova et al., 2020). Therefore, dopants' addition may manipulate the TiO₂ main features such as surface area, recombination rate, bandgap energy level, optical and other traits (Khlyustova et al., 2020). For example, recent research shows that zinc oxide ZnO (wurtzite); has higher chemical stability, good electron activity at room temperature, non-toxicity, and has a broader bandgap energy (3.2 eV) compared to TiO₂ phases¹¹. However, single usage of ZnO also has limitations, such as the recombination rate of electrons and holes difference and photosensitivity¹². However, the coupling of semiconductor oxides provides enhanced redox reactions that create increased photocatalytic activity. In addition, coupling TiO₂ with ZnO tend to enhance chemical stability and change the recombination rate of electron and holes¹³. Furthermore, the difference in valence and conduction band of TiO₂ and ZnO generates a more stable conductivity¹⁴. In the antibacterial inhibition part, providing a redox reaction increases the antibacterial inhibition because of the ROS generations¹⁵. These features of ZnO doped TiO₂ thin films may provide enhanced optical, structural, and antibacterial activity. In the production of TiO₂, various methods can be helpful, but the most important thing is time and money consumption. Recently, most of the technological advancement done by the nano-thickness scale and these materials provide various biomedical, electrical, physical, and chemical abilities. These new properties can be beneficial for bioactivity. The introduction of thin films on bioactivity can be beneficial for various applications. A single or multilayer creates these films and their thickness changes from nanometers to a few micrometers. These thin films contain two parts: the substrate and the layer part. These thin films provide various functions to execute against microorganisms, such as material transformation on wastewater's harmful environment or biodegradation. Due to these unique functionalities, the preparation of thin films is crucial for the outcome. Different deposition techniques are viable in thin-film production, such as physical and chemical depositions¹⁵⁻²¹. In this study, the sol-gel method was chosen as a preparation technique since the sol-gel method is a beneficial deposition technique to obtain a thin film for several different usage areas such as biomedical, chemical and electrical¹⁸ and its unique traits such as homogeneity, sustainability, effectiveness, and low cost²².

Homogeneity is crucial for this experiment because this experiment mainly focused on comparison of ZnO doped TiO₂ thin films with pure TiO₂ thin films.

2. MATERIALS AND METHOD

2.1. Production of Brookite Phase

The nanostructured TiO₂ sol was prepared using a mixture of titanium tetra isopropoxide (Ti [OCH(CH₃)₂]₄; (TTIP) Sigma-Aldrich), nitric acid (HNO₃), deionized water (DI), and isopropanol. First, titanium tetra isopropoxide (TTIP) was dissolved in isopropanol. Nitric acid was added dropwise in the solution under continuous stirring. Deionized water was added for hydrolysis. As a solution of TTIP:isopropanol:DI:AcAc a volume ratio of (0.4:4:0.1:0.2) was used. The solution was mixed using magnetic stirring for three hours at a room temperature of 22 °C.

2.2 Production of Anatase Phase

Titanium tetra isopropoxide (Ti [OCH(CH₃)₂]₄; (TTIP) was mixed with acetic acid and ethanol with a molar ratio of 0.08:0.48:4, respectively. The mixture was stirred for two hours at a room temperature of 22 °C.

2.3 Production of Rutile Phase

Tetrabutyl orthotitanate (Ti (OCH₂CH₂CH₂CH₃)₄; TBOT) was dissolved in ethanol under vigorous stirring for 30 minutes. Then, in another beaker, ethanol was mixed with Hydrochloric acid (HCl) for 30 minutes. Afterward, the second solution in the other beaker was slowly added dropwise to the first solution under vigorous stirring until homogeneous. Then, preparation of the TiO₂ films with various crystal phases, the solutions prepared by the sol-gel process were spin-coated on the corning 2947 substrates. Next, the films were heat-treated at 450 °C for one hour, for brookite and anatase crystal phases, at 600 °C for the rutile crystal phase. After the heat treatment, one layer was formed on the surface of the films. Then, the films were coated with a spin coater again, paying attention to the TiO₂ solution coated side on the upper surface, and heat treatment and spin coating processes were continued until the films were 3-layered.

2.4 Production of ZnO (wurtzite)

The solution was prepared by dissolving zinc acetate dehydrate (ZnAc) in isopropanol. Dea (Diethanolamine), which is a surface-active material, is used to accelerate solving. Water was added for hydrolysis reactions, as a precursor solution of ZnAc:isopropanol:Dea: water, a volume ratio of 0.4:4:0.1:0.2 was used. The solution was mixed using magnetic stirring for one hour at 60°C.

2.5 Production of ZnO/TiO₂ material

The obtained solution in Section 3.1.4 was mixed with one of the leading TiO₂ solutions for brookite, rutile, or anatase phase at ZnO/TiO₂ volume ratios of 0, 0.01, 0.02, 0.05, 0.1, denoted as ZTA0-10, ZTB0-ZTB10, ZTR0-ZTR10, respectively. The final solutions were deposited on corning 2947 glass substrates by spin-coating deposition (1000 rpm/30 s), using a spin coater at room temperature (22°C). After coating, ZnO films were immediately placed in a microprocessor controlled (CWF 1100) furnace, heated at 450°C. The films were taken out of the furnace and left at room temperature at the end of 1 hour. Finally, all coatings and heat treatment processes were repeated two times to get three-layered films.

2.6 Optical Properties and Homogeneity Studies

Ultraviolet-visible (UV-vis) spectrophotometer is an absorbance determination material used to understand materials' optical features in solution or solid phase. This device tracks the excited atoms by looking at their wavelength and absorbance energies. UV-vis spectrophotometer detects the absorbance of the film between the range of 200-1100 nm spectrum. The absorbance value is calculated by Beer-Lambert law (Equation 1).

$$A = \log_{10} (I_0/I) = \epsilon bc, \quad (1)$$

For the single wavelength, A is absorbance (unitless), ϵ is known as a molar absorptivity (molar, M⁻¹cm⁻¹), b is the length of the path (cm), c is solution concentration (M), I_0 is the intensity of light at a specific wavelength, and I is the transmitted intensity. Moreover, UV-vis spectroscopy can provide quantitative and qualitative information about samples.

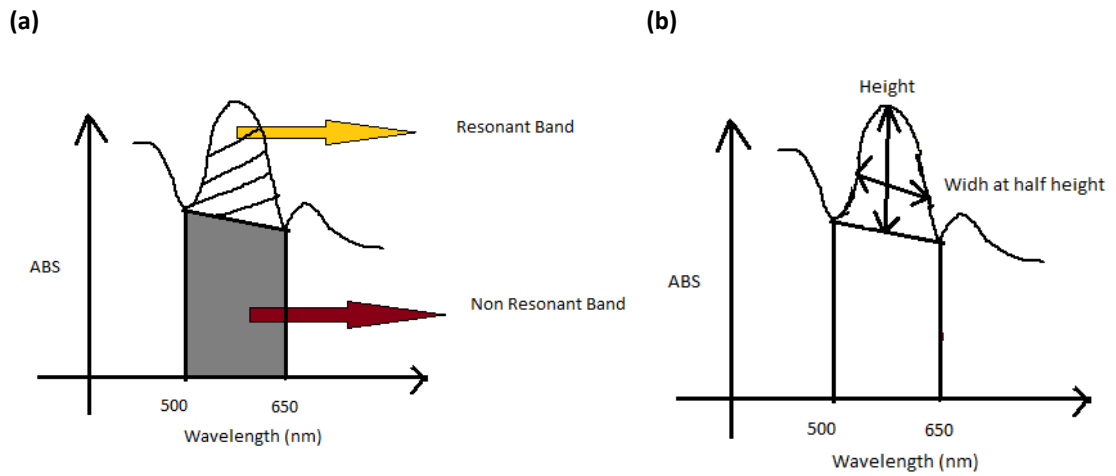


Figure 1. (a) Representation of resonant and non-resonant band (b) Representation of Height and Width at half height (FWHM)

In UV-vis spectrophotometric analysis' the most crucial part is finding the area under the curve because the area under the curves gives the resonance ratio. The resonance ratio is an essential concept for homogeneity, and it has been calculated by dividing the resonant band area into a non-resonant band area. In addition, another critical concept called normalized width is calculated by the division of width of the resonant band into the height of the resonant band-both resonance ratio and normalized width is essential for optical analysis of materials ³⁰.

$$\text{Resonance ratio} = \text{Area of resonant band} / \text{area of the nonresonant band} \quad (2)$$

$$\text{Normalized width} = \text{Width of resonance band} / \text{height of the resonant band} \quad (3)$$

2.7 XRD Analysis

XRD is a widely used analytic method for physical and chemical composition identification. XRD instruments include three elements: a sample holder, an X-ray detector, and an X-ray tube. Generally, cathode tubes create the X-ray and voltage applied for accelerating the electrons than electrons bombarding the target material. Therefore, the XRD is a helpful method for analyzing homogeneity, crystal property, and average particle size. In general, XRD creates monochromatic X-rays, and these X-rays are

scattered at specific angles to create specific peaks according to a sample's crystalline structure 31.

Every material has a unique set of d-spacing which means converting diffraction peaks to d-spacing reveals the type of the material. Due to these traits, the XRD pattern reveals the atomic composition of the material. Moreover, XRD analysis provides the atomic position of the crystalline structure. XRD analysis application on thin films provides information about lattice formation between substrate and film, homogeneity of materials, quality of the film, thickness, and toughness of the thin film. The XRD result shows the average crystal size using Scherrer's equation (Equation 4).

The particle diameter size of different thin films was calculated according to Equation 4:

$$D = \frac{K \lambda}{B \cos \theta} \quad (4)$$

In Equation 4, D represents the diameter of the TiO₂ nanocrystals, K presents the shape factor, and it has a constant value (0.89), λ represents the radiation wavelength, B represents the full width at half maximum (FWHM) of the diffraction line, and θ (theta) represents the Bragg angle (rad)³².

2.8 Antibacterial Measurement

The antibacterial activity of TiO₂ is crucial for biodegradation, wastewater remediation and antibacterial disinfection. TiO₂ thin films used various applications related to antibacterial activity. The advantages of TiO₂ are photocatalytic activity, high degradation efficiency and non-toxicity³³. Due to these traits, TiO₂ thin film can provide a suitable solution for antibacterial disinfection studies. Antibacterial materials have rapidly grown in recent years, and most technological advancements need to provide antibacterial traits. Therefore, the ISO 22196 method was used to determine the antibacterial activity of TiO₂ thin films. In addition, ISO 22196 is a method that quantitatively evaluates the antibacterial activity (growth inhibition or killing) of samples such as plastic, other non-porous, and surface products (ICS, 2011). Therefore, ISO 22196 is an excellent method to determine bacteriostatic (growth inhibition) and bactericidal (killing bacteria) features, and this test is highly critical for TiO₂ usages for future technologies. Different types of pure and doped TiO₂ thin film antibacterial efficiencies were represented (Table 1).

Table 1. Antibacterial efficiency of different types of Pure TiO₂ and doped TiO₂

Thin Film type	Bacteria type	Light Source	Highest Antibacterial inhibition %	References
Sn ⁴⁺ - TiO ₂ film	<i>E. coli</i> , <i>S.aureus</i>	UV	99.9%	34
TiO ₂ film	<i>S.aureus</i> , <i>S.epidermidis</i> , <i>E.coli</i>	UV	47 %	35
TiO ₂ /Ag/Cu	<i>E. coli</i>	UV	100%	36
Mg- TiO ₂ thin film	<i>E. coli</i> <i>Pseudomonas</i> <i>Bacillus sp</i> <i>Staphylococcus</i>	UV	100%	37
Cu-doped TiO ₂ thin film	<i>Phytophthorapalmivorahas</i>	UV	75% but concentrations >3% kill % 100	38
Ag- TiO ₂ /PDMS thin film	<i>M.luteus</i> <i>S.maltophilia</i>	Visible irradiation	100%	39
ZnO(wurtzite), TiO ₂ , and ZnO- TiO ₂ thin films	<i>A.flavusthan</i>	UV	100%	40

Surfaces needed to be smooth, 1cm thick, and 5x5 cm² shapes. Six samples of a corning glass covered with thin films were prepared for the experiment; three samples were to test bacteria and three to control groups. Each of these samples (TiO₂, ZnO/TiO₂) was analyzed by ISO 22196.

In antibacterial analysis, gram-positive “*Staphylococcus aureus*” and gram-negative “*Escherichia coli*” were used. The antibacterial activity of the films was evaluated by colony-forming unit (CFU) counting. After incubation, the colonies were counted. CFU per ml was calculated for each sample at different time intervals (0-120 min) by using the following formula:

$$\text{CFU/ml} = \text{No. of colonies} \times \text{Dilution factor} / \text{volume inoculated} \quad (5)$$

2.9 Characterizations

The absorbance spectra of composite films were measured using Labomed Spectro 22 UV–vis Spectrophotometer in the spectral range of 190–1100 nm wavelengths. The calculations of under the curve area, the entire width of half maximum of the absorbance data were performed by Origin 8.0 Software focusing the absorbance peak regions. The optical band gap energies of the composite films were calculated from the Tauc Plot since the thickness of the films was suitable for applying Beer-Lambert’s Law. An X-ray diffractometer (XRD, Philips PW-1800) with Cu-K α radiation (The wavelength of Cu-K α is 0.15406 nm) was used to identify the films' crystal phases. The antibacterial response of the films was investigated using gram-positive “*Staphylococcus aureus*” (*S. aureus*) and gram-negative “*Escherichia coli*” (*E. coli*) according to the standard of ISO 22196. The initial dose of these bacteria’s concentration was 10⁵CFU/ml. Since TiO₂ shows antibacterial properties under UV light exposure and its photocatalytic effect is known, the antibacterial effect in the visible light region was investigated by doping with ZnO.

3. RESULTS AND DISCUSSION

3.1 XRD Results

The most crucial thing in the calculation is the theta value. Generally, theta value is found with two thetas and must convert a single theta value to determine the diameter of particles properly. Then, the calculation and comparison of the XRD values were determined (Table 2).

Table 2. XRD values of different types of thin films and their diameter size

Thin films	K	$\lambda(\text{Å})$	Peak positions 2θ	FWHM	D(nm)
TiO ₂ (anatase)	0.89	1.54	25.27	0.36	21.85
TiO ₂ (brookite)	0.89	1.54	31.58	0.16	50.18
TiO ₂ (rutile)	0.89	1.54	27.30	0.21	36.89
ZTA0(1 st Peak)	0.89	1.54	25.27	0.36	21.85
ZTA0(2 nd Peak)	0.89	1.54	37.69	0.34	24.19
ZTA1(1 st Peak)	0.89	1.54	25.23	0.31	25.87

ZTA1(2 nd Peak)	0.89	1.54	37.66	0.25	32.05
ZTA2 (1 st Peak)	0.89	1.54	25.21	0.36	21.77
ZTA2 (2 nd Peak)	0.89	1.54	37.67	0.25	32.12
ZTA5	0.89	1.54	25.19	0.43	18.66
ZTA10(1 st Peak)	0.89	1.54	25.22	0.34	23.45
ZTA10(2 nd Peak)	0.89	1.54	37.68	0.33	24.75
ZTA10(1 st Peak)	0.89	1.54	25.23	0.31	25.87
ZTA10(2 nd Peak)	0.89	1.54	37.66	0.25	32.05
ZTA10(3 rd Peak)	0.89	1.54	25.21	0.36	21.77
ZTA10(4 th Peak)	0.89	1.54	37.67	0.25	32.12
ZTB0	0.89	1.54	31.58	0.16	50.18
ZTB1	0.89	1.54	31.54	0.35	23.07
ZTB2	0.89	1.54	31.55	0.34	23.97
ZTB5	0.89	1.54	31.60	0.48	16.98
ZTB10	0.89	1.54	31.76	0.59	13.61
ZTR0	0.89	1.54	27.30	0.21	36.89
ZTR1(1 st Peak)	0.89	1.54	27.30	0.24	33.22
ZTR1(2 nd Peak)	0.89	1.54	36.18	0.55	14.93
ZTR2(1 st Peak)	0.89	1.54	27.30	0.21	36.96
ZTR2(2 nd Peak)	0.89	1.54	36.08	0.25	32.86
ZTR5	0.89	1.54	27.30	0.21	37.21
ZTR10(1 st peak)	0.89	1.54	36.08	0.28	29.49
ZTR10(2 nd Peak)	0.89	1.54	25.76	5.58	1.44
ZTR10(3 rd Peak)	0.89	1.54	31.59	0.92	8.85
ZTR10(4 th Peak)	0.89	1.54	34.40	0.62	13.08
ZTR10(5 th Peak)	0.89	1.54	36.19	0.64	12.73
ZnO(1 st Peak)	0.89	1.54	31.75	0.15	52.87
ZnO(2 nd Peak)	0.89	1.54	34.55	0.16	50.56
ZnO(3 rd Peak)	0.89	1.54	36.44	0.16	51.11

In this study, decreased size diameter needs to be achieved after using ZnO as a dopant material. The average particle size of ZnO was found at 51.51 nanometers. The average size of pure TiO₂ phases anatase was at 21.86 nm, brookite was at 50.18 nm, and rutile was at 36.9 nm. ZnO doped anatase TiO₂ (ZTA) XRD data shows that a small concentration of ZnO doped increases the diameter size of TiO₂ then decreases the composite size slowly after adding more ZnO concentration. In ZnO doped brookite TiO₂ (ZTB), XRD data shows that adding every ZnO into brookite decreases the diameter size due to brookite orthomorph structure. ZnO doped rutile TiO₂ XRD data shows that the addition of ZnO also decreases the average particle size of pure slowly. This slow increase and decrease of particle size in ZTR (doped rutile) and ZTA (doped anatase) is related to their tetragonal structure. Symmetrical structure affects the bond formation and hindering.

Figure 2 (a) shows that the films have a rare brookite phase, an orthorhombic crystal structure. A single crystallization peak (211) of the brookite phase at a 2θ value of 31.5° corresponds to ICDD Card No. 04-019-9878. In Figure 2 (c), the sharp diffraction peaks at 25.2° , 37.7° , and 47.8° theta values are indexed to the (101), (004), and (200). Planes of the anatase phase of TiO_2 correspond to 21-1272 according to ICDD Card. In Figure 2 (d), the peaks at the 2θ values of 27.31° , 36.12° , and 41.25° are fitted well with the (110), (101), and (111) planes of the rutile phase of TiO_2 (ICDD Card No. 21-1276), respectively. These (anatase and rutile) are tetragonal phases of TiO_2 .

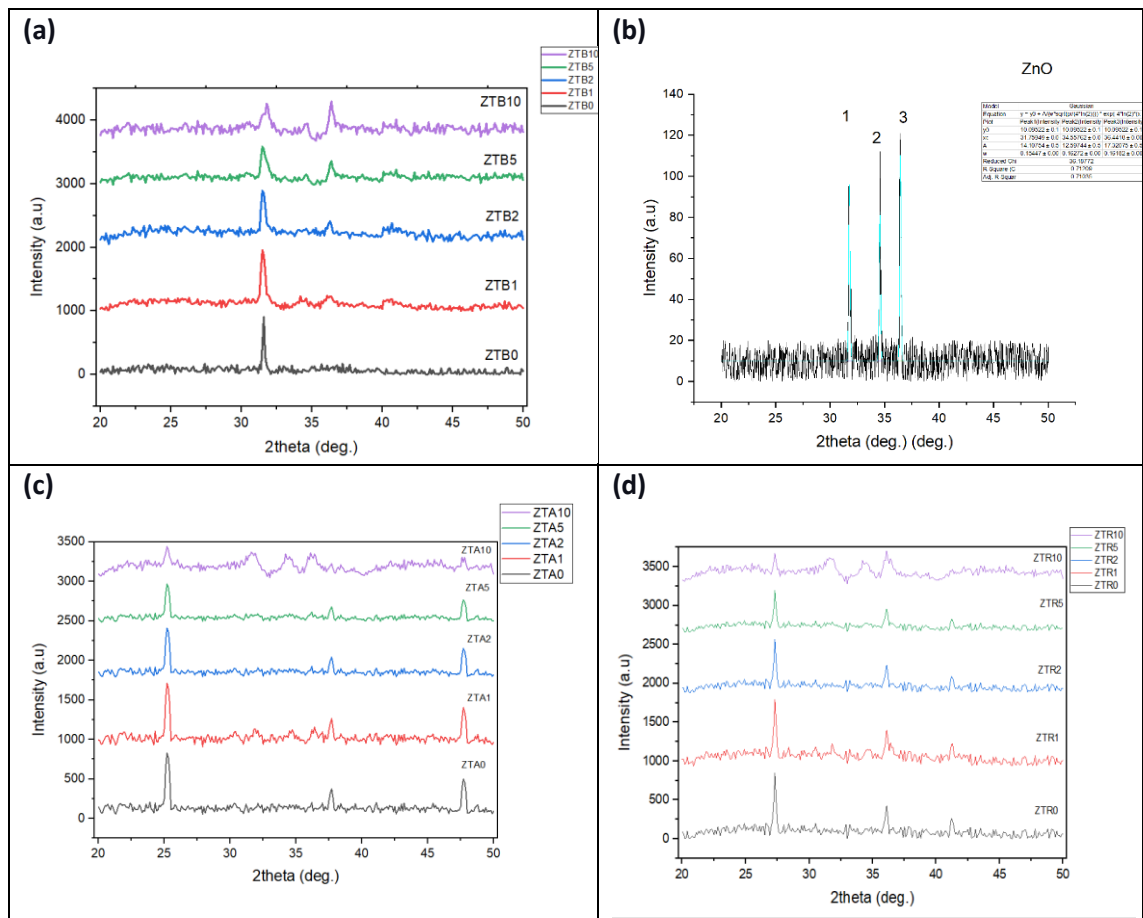


Figure 2. XRD response of (a) ZnO doped TiO_2 brookite films with various ZnO/ TiO_2 doping ratios, (b) ZnO film and parameter calculations, (c) ZnO doped TiO_2 anatase films with various ZnO/ TiO_2 doping ratios, (d) ZnO doped TiO_2 rutile films with various ZnO/ TiO_2 doping ratios.

3.2 Optical Characteristics of the Films

Absorption spectra of pure TiO₂ films and ZnO doped TiO₂ films were analyzed using UV-vis spectrophotometers, as shown in Figure 3. High absorbance values are seen between at 200-500 range. According to absorbance-wavelength graphs, the addition of ZnO can enhance the absorbance rate of all three phases. On the other hand, the high absorbance value of ZnO can decrease the absorbance range of Pure TiO₂ phases because dilution of pure TiO₂ absorbance ability reduces, and the addition of ZnO introduces its photon absorbance rate. Recombination of rate increases, and absorption of doped nanocomposites decreases. The addition of ZnO also affects the resonance ratio and homogeneity of the material. Doped material may enhance the photocatalytic activity, but the optimum amount of dopant addition is so important for homogeneity concerns. A comparison of different volumes of ZnO doped anatase, brookite, and rutile was determined (Figure 3 to 6). In normal conditions, the material homogeneity is determined by the relation between resonance ratio and normalized width. When the resonance ratio increases and normalized width decreases, that implies composites reach a more homogenous structure. According to calculations, adding ZnO dopant decreases the resonance ratio and increases the normalized width, which is vice versa of literature information. However, our studies do not ultimately increase or decrease; some ranges in which composites resonance ratio increases with ZnO. This result provides good information, such as the critical point to cut down dopant addition to getting the more homogenous structure. Further studies can arrange their dopant addition to these ranges to get more homogenous material. ZTA5-10, ZTB5-10, and ZTR5-10 concentration ranges are critical for the homogeneity shift for excessive dopant addition (Table 3).

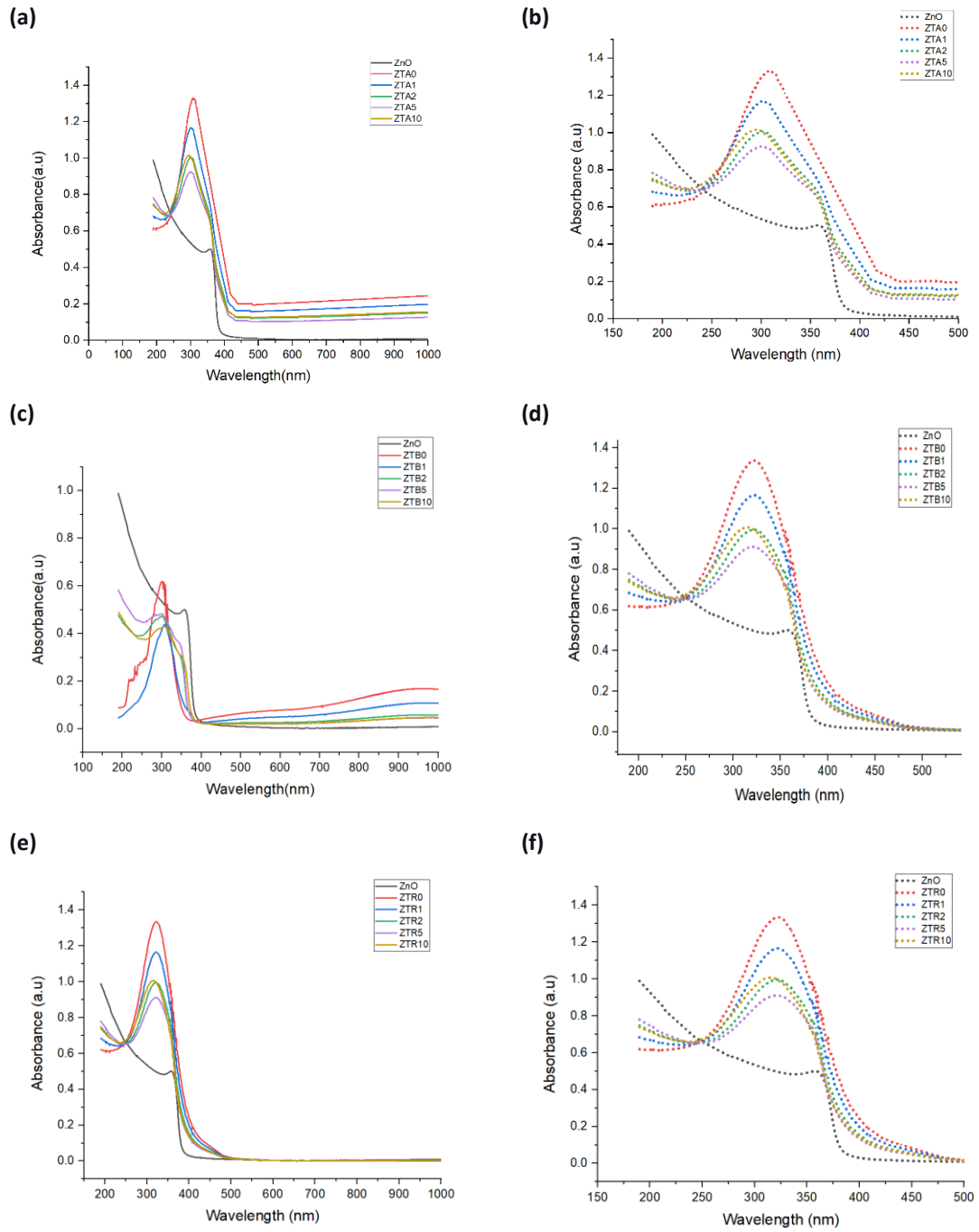


Figure 3. Absorbance wavelength spectrum of ZnO and ZnO doped TiO₂. In (a-c-e) graphs show the range between 200-1000 spectrum, and (b-d-f) graphs show the detailed range between 200-500 range spectrum.

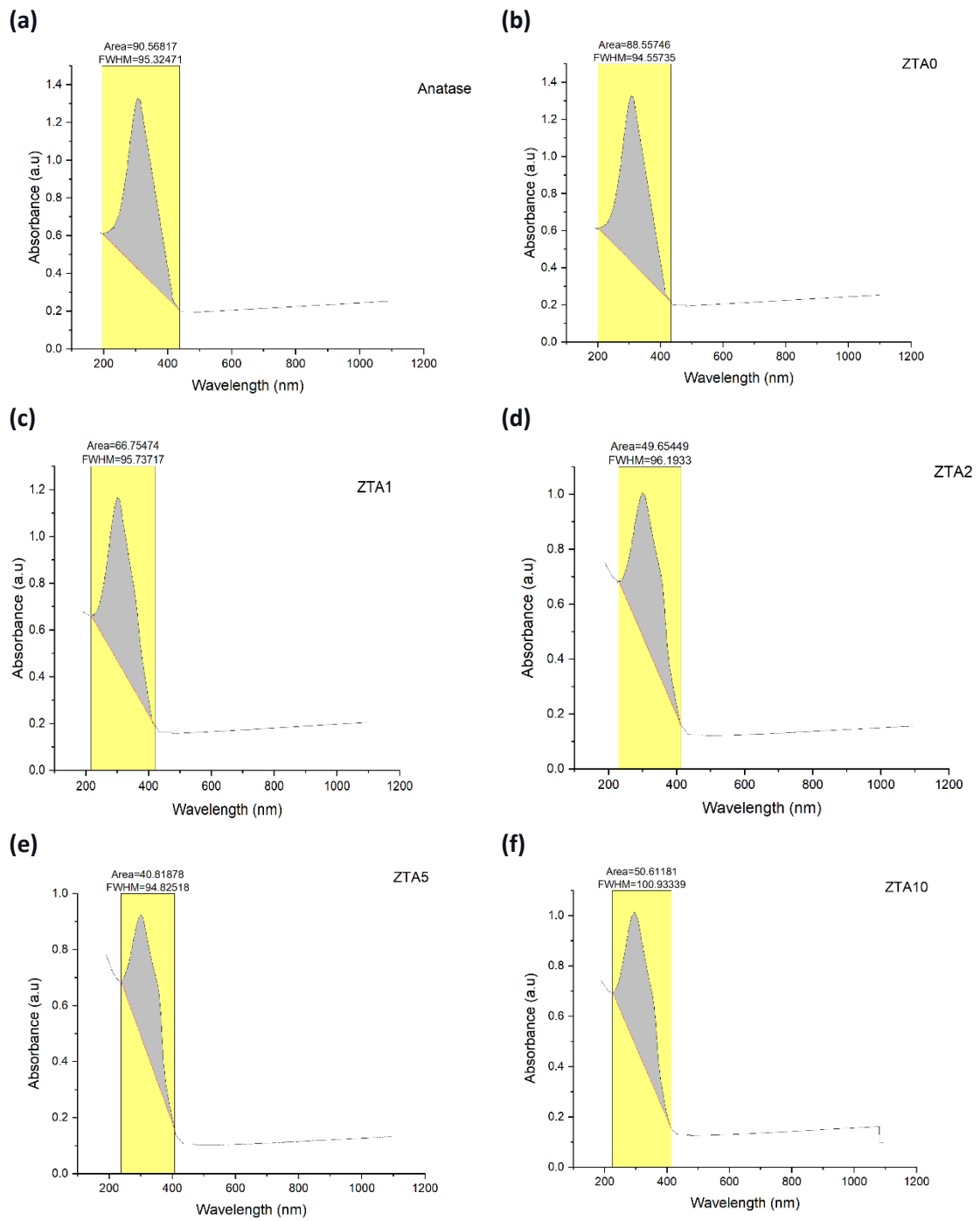


Figure 4. Resonant band representation of pure (a) and ZnO doped (b-f) anatase TiO_2

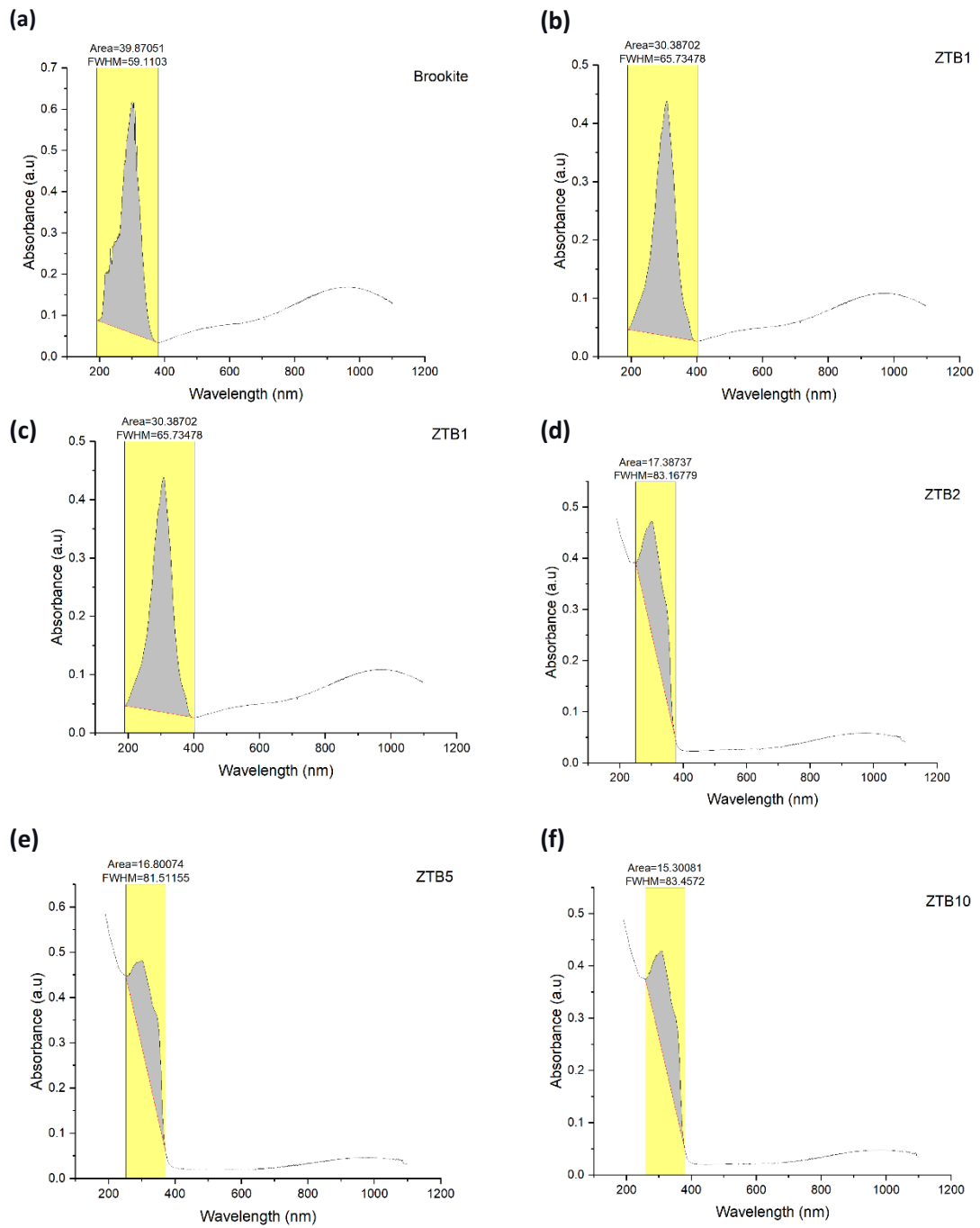


Figure 5. Resonant band representation of pure (a) and ZnO doped (b-f) brookite TiO₂

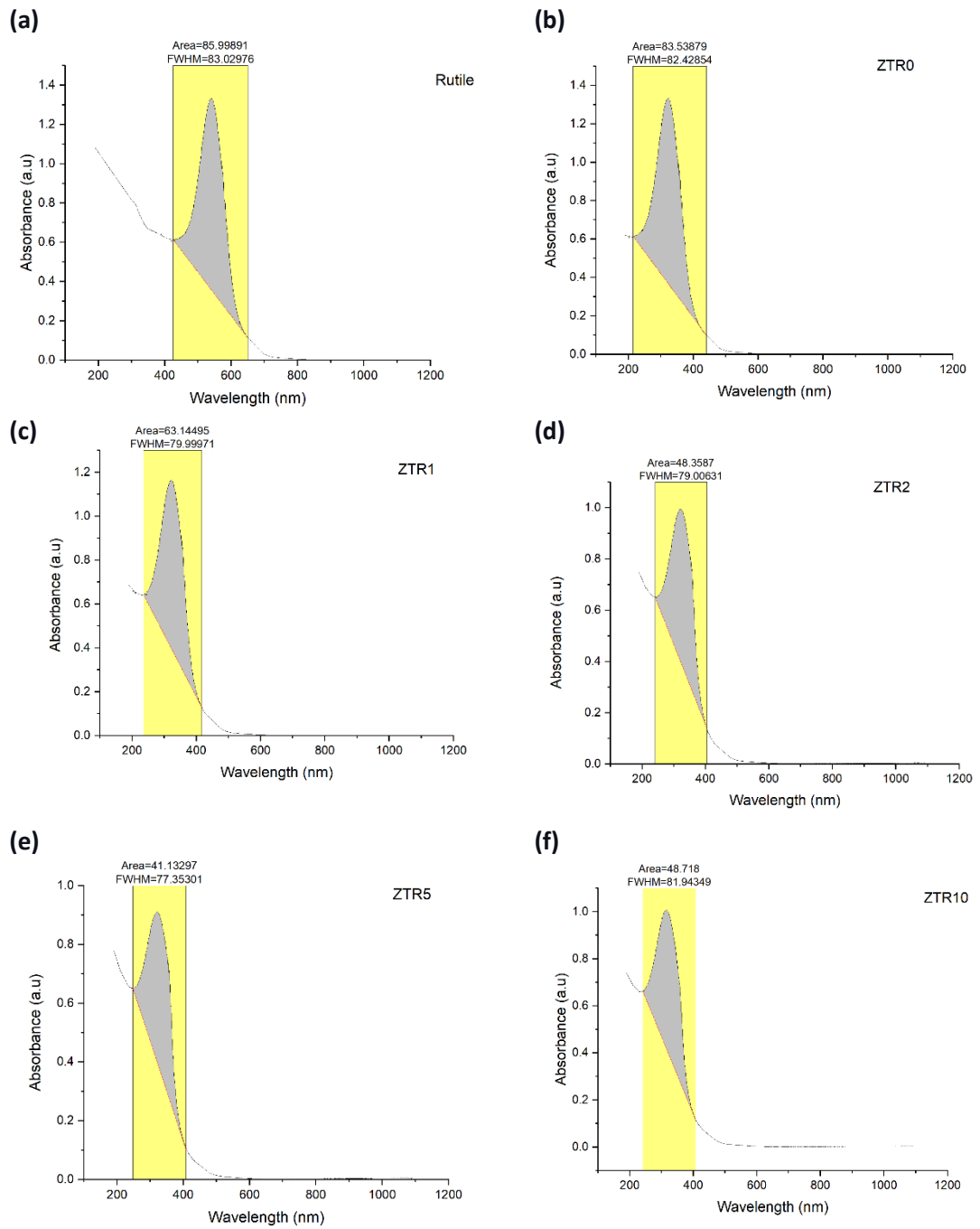


Figure 6. Resonant bands representation of pure (a) and ZnO doped (b-f) rutile TiO₂.

In-band energy analysis, the Tauc pilot measured materials' band-gap energies (Equation 6).

$$(\alpha h\nu) = B (h\nu - E_g)^r \quad (6)$$

Table 3. Calculation of resonance ratio and normalized width of pure and ZnO doped TiO₂

Thin films	Area of resonant band	Area of non-resonant background	Resonance ratio	Width of resonant band	Height of resonant band	Normalized width
Pure TiO ₂ (anatase)	90.56	100.52	0.90	95.32	0.90	104.97
Pure TiO ₂ (brookite)	39.87	11.46	3.47	59.11	0.56	105.15
Pure TiO ₂ (rutile)	85.99	87.29	0.98	83.02	0.98	84.11
ZTA0	88.55	97.13	0.91	94.55	0.89	105.14
ZTA1	66.75	87.41	0.76	95.73	0.70	135.66
ZTA2	49.65	77.41	0.64	96.19	0.53	180.24
ZTA5	40.81	72.15	0.56	94.82	0.44	212.55
ZTA10	50.61	80.79	0.62	100.93	0.52	191.56
ZTB0	39.90	11.34	3.51	59.13	0.56	105.20
ZTB1	30.38	7.75	3.91	65.73	0.40	163.06
ZTB2	17.38	27.52	0.63	83.16	0.22	364.62
ZTB5	16.80	30.29	0.55	81.51	0.21	378.41
ZTB10	15.30	35.76	0.42	83.45	0.19	431.66
ZTR0	83.53	81.09	1.03	82.42	0.96	85.17
ZTR1	63.14	70.08	0.90	79.99	0.77	103.60
ZTR2	48.35	64.85	0.74	79.00	0.60	130.06
ZTR5	41.13	60.50	0.67	77.35	0.52	146.87
ZTR10	48.71	64.83	0.75	81.94	0.60	136.11

In general, Titanium dioxide (TiO₂) is an excellent semiconductor in terms of bandgap energy, such as anatase 3.20 eV, rutile 3.00 eV, and brookite 3.13 eV⁴⁻⁶. The photocatalytic ability of pure TiO₂ and ZnO doped TiO₂ was determined. In a normal condition, ZnO addition needs to increase the bandgap energy of pure TiO₂, but TiO₂ is an indirect semiconductor, and ZnO is a direct conductor. Thus, every possible indirect and direct graph needs to be evaluated for optimum results (Figure 7). These graphs find from the absorbance value of every single material. In direct conduction, the r variable equals two, and the indirect conduction r variable equals to 1/2. After creating their Tauc plots, ZnO doped anatase tends to be a direct conductor, ZnO doped brookite tends to the indirect conductor, and ZnO doped rutile tend to act like a direct conductor. Discrimination of indirect and direct conduction is done by using the Tauc plot. ZnO normal bandgap energy around at 3.37 eV¹¹. The addition of ZnO dopant needs to increase the original bandgap energy of pure TiO₂ phases. Due to this reason, (a), (d), (e)

in Figure 7 shows that the addition of ZnO dopant increases the original band gap energy of TiO_2 .

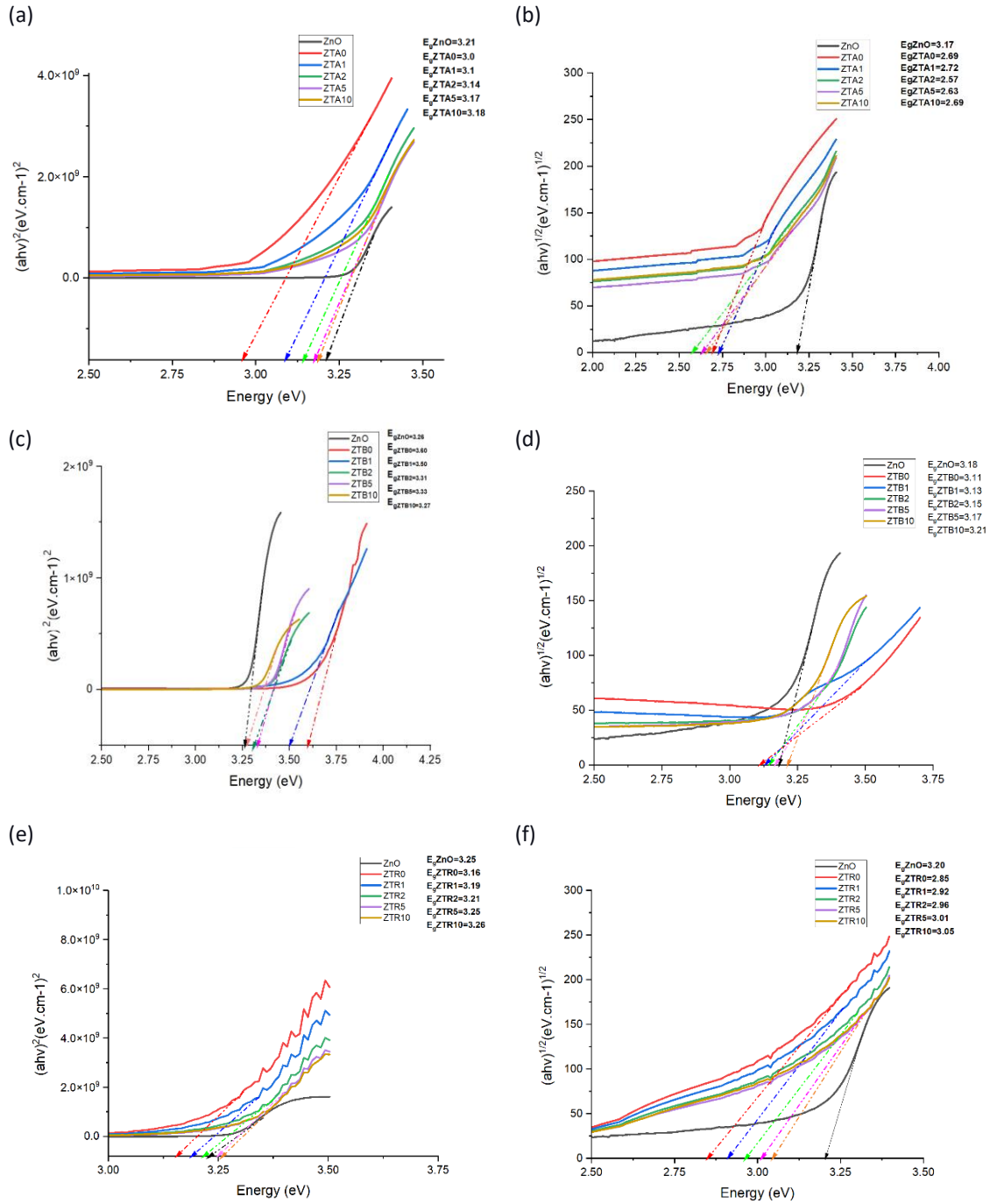


Figure 7. Tauc Plot of pure ZnO and ZnO doped Anatase, Brookite, and Rutile phases of TiO_2 with various ZnO/ TiO_2 ratios. The extrapolation of the curves shows the optical energy band gap of ZTA, ZTR, and ZTB.

Table 4. Bandgap energy values of different types of doped material derived from the Tauc plot.

Film type	Direct(eV)	Indirect(eV)
ZnO	3.21	3.17
ZTA0	3.0	2.69
ZTA1	3.1	2.72
ZTA2	3.14	2.57
ZTA5	3.17	2.63
ZTA10	3.18	2.69
ZTB0	3.60	3.11
ZTB1	3.50	3.13
ZTB2	3.31	3.15
ZTB5	3.33	3.17
ZTB10	3.27	3.21
ZTR0	3.16	2.85
ZTR1	3.19	2.92
ZTR2	3.21	2.96
ZTR5	3.25	3.01
ZTR10	3.26	3.05

3.3 Antibacterial Activity

Figure 8 presents the antibacterial response of films with respect to the time for *E. coli* and *S.aureus*. *E. coli* count reduced from 10^5 to 10^4 with 120 min of irradiation time for pure brookite TiO₂ film. A dramatic decrease in the bacteria number for both bacteria was observed for ZnO/TiO₂ composite films compared with TiO₂ films under the lighting with visible light. After 120 min. of light exposure, the bactericidal survival decreases of ZTA0, ZTA1, ZTA2, ZTA5, and ZTA10 films against *E. coli* were 10^0 , 3×10^1 , 10^2 , 2×10^2 and 7×10^3 , respectively. Meanwhile, exhibiting a similar trend, the bactericidal survival decreases of ZTA0, ZTA1, ZTA2, ZTA5, and ZTA10 films against *S. aureus* were 10^0 , 5×10^1 , 2×10^2 , 6×10^3 and 10^4 , respectively. For ZTB2-ZTB10 films, complete inactivation of the *E. coli* was recorded at 120, 90, and 75 min of light exposure, respectively. Since TiO₂ shows antibacterial properties under UV light exposure and its photocatalytic effect is known, the antibacterial effect in the visible light region was investigated by doping with ZnO. These results show that the content of ZnO in the ZnO/TiO₂ composite films plays a significant role for enhancing the antibacterial activity of the films in the absence of UV light.

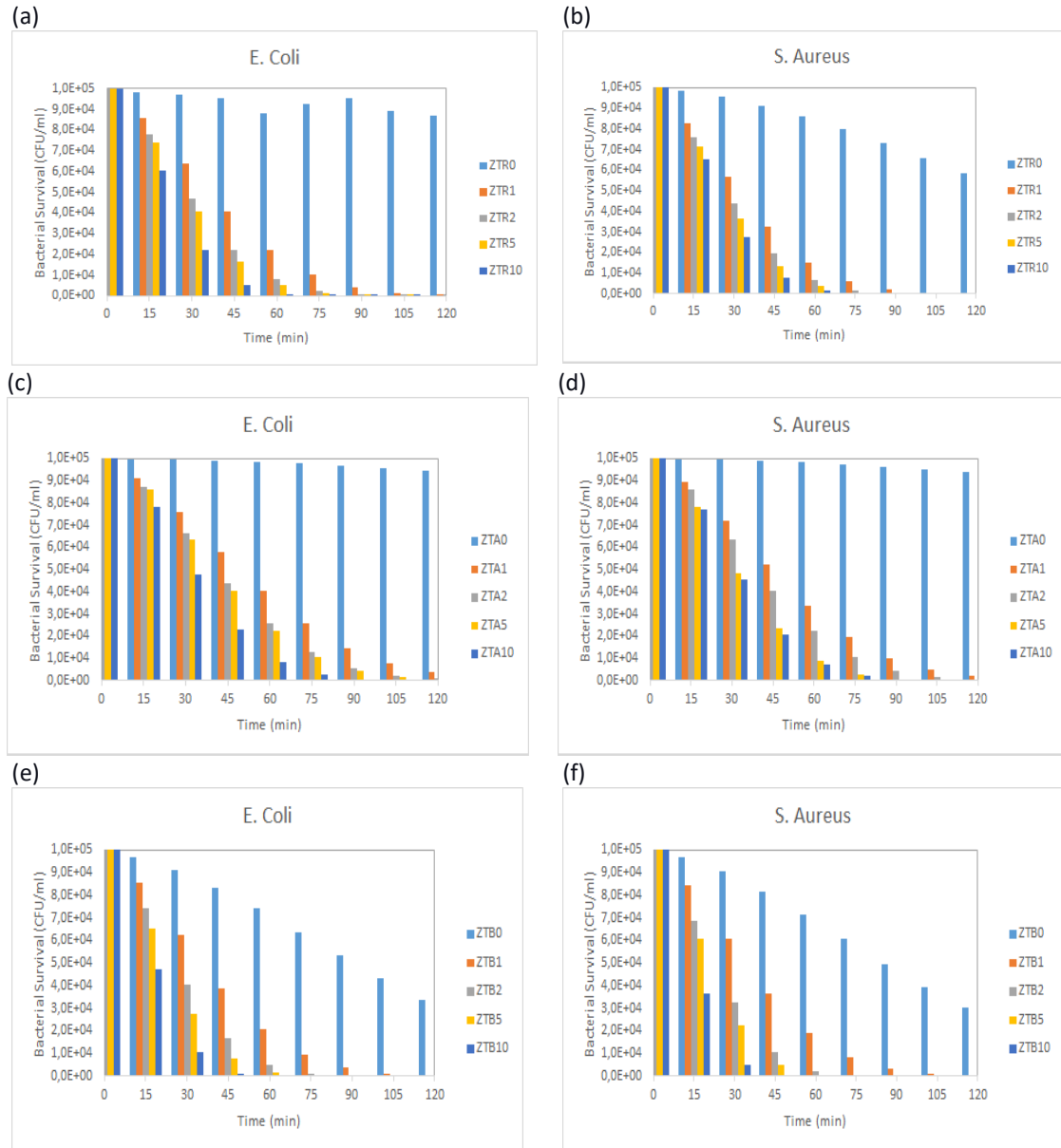


Figure 8. Antibacterial response of ZnO doped Anatase, Brookite, and Rutile phases of TiO₂ with various ZnO/TiO₂ ratios under light exposure for *E. Coli* and *S. Aureus*.

4. CONCLUSION

In conclusion, XRD results show that the particle size of TiO₂ can be reduced in the brookite phase rather than anatase and rutile due to brookite's large volume. However, anatase and rutile also show remarkable diameter size drop when the concentration is appropriately arranged. However, the ZTA5 sample is also a good concentration for

anatase applications. Due to their structural stability traits, anatase and rutile particle size decrease slowly. UV data show that the resonance ratio is essential for cell homogeneity and dispersibility. Due to this reason addition of dopant materials needs to be controlled by stoichiometry for optimum homogeneity. Using the sol-gel method provides the minor homogeneity range for a concentration of doped ZTA5-10, ZTB5-10, and ZTR5-10. In these concentration ranges, particles size dropping and their antibacterial activity increases. Band gap energy enhancement of ZnO was shown by using the Tauc plot. In addition, direct ZnO doped anatase TiO₂, direct ZnO doped rutile and indirect ZnO doped brookite conduction bands were determined. In antibacterial inhibition, after 105 minutes, all of the bacterial growth inhibited against *E.coli*. After 90 minutes, all of the bacterial growth inhibited against *S.Aureus* in the rutile phase. After 120 minutes, most bacterial growth inhibited beside ZTA1 against *E.coli* and *S.Aureus* in the anatase phase. Finally, after 75 minutes, most bacterial growth inhibited beside ZTB1 against *E.coli* and *S.Aureus* in the brookite phase. This research mainly focused on discovering how dopant material can enhance the activity of pure material and how these enhanced traits can be used on optical and antibacterial activity. Therefore, ZnO/TiO₂ composite films can give an alternative solution for antibacterial surface applications under visible light.

REFERENCES

1. Gossen, L. and L. Velichkina, *Environmental problems of the oil-and-gas industry*. Petroleum Chemistry, 2006. **46**(2): p. 67-72.
2. Menazea, A. and N.S. Awwad, *Antibacterial activity of TiO₂ doped ZnO composite synthesized via laser ablation route for antimicrobial application*. Journal of Materials Research and Technology, 2020. **9**(4): p. 9434-9441.
3. Ahmed, M., et al., *Composition and design of nanofibrous scaffolds of Mg/Se-hydroxyapatite/graphene oxide@ ε-polycaprolactone for wound healing applications*. Journal of Materials Research and Technology, 2020. **9**(4): p. 7472-7485.
4. Linsebigler, A.L., G. Lu, and J.T. Yates, *Photocatalysis on TiO₂ Surfaces: Principles, Mechanisms, and Selected Results*. Chemical Reviews, 1995. **95**(3): p. 735-758.
5. Thiyagarajan, D., R. Sivakumar, and I. Rajangam, *Growth of micro flower rutile TiO₂ films by chemical bath deposition technique: Study on the properties of structural, surface morphological, vibrational, optical and compositional*. Surfaces and Interfaces, 2016. **4**.
6. Wang, Y., et al., *Review of the progress in preparing nano TiO₂: an important environmental engineering material*. J Environ Sci (China), 2014. **26**(11): p. 2139-77.
7. Luttrell, T., et al., *Why is anatase a better photocatalyst than rutile?--Model studies on epitaxial TiO₂ films*. Sci Rep, 2014. **4**: p. 4043.
8. I M Joni, L.N.a.C.P., *Characteristics of TiO₂ particles prepared by simple solution method using TiCl₃ precursor*. Journal of Physics: Conf. Series, 2018.
9. Zhang, H. and J.F. Banfield, *Structural characteristics and mechanical and thermodynamic properties of nanocrystalline TiO₂*. Chem Rev, 2014. **114**(19): p. 9613-44.
10. Kumar, R.S., et al., *Synthesis, characterization, and photocatalytic disinfection studies of porphyrin dimer/TiO₂-based photocatalyst*. Journal of Molecular Structure, 2021. **1236**.
11. Firdaus, C.M., et al., *Characterization of ZnO and ZnO: TiO₂ Thin Films Prepared by Sol-Gel Spray-Spin Coating Technique*. Procedia Engineering, 2012. **41**: p. 1367-1373.
12. William IV, L., et al., *Impact of heat treatment and composition of ZnO– TiO₂ nanoparticles for photocatalytic oxidation of an azo dye*. Industrial & engineering chemistry research, 2008. **47**(5): p. 1483-1487.

13. Habib, M.A., et al., *Synthesis and characterization of ZnO-TiO₂ nanocomposites and their application as photocatalysts*. Int. Nano Lett., 2013. **3**(1): p. 1-8.
14. Cho, S., et al., *Research Update: Strategies for efficient photoelectrochemical water splitting using metal oxide photoanodes*. Apl Materials, 2014. **2**(1): p. 010703.
15. Stoyanova, A., et al., *Synthesis and antibacterial activity of TiO₂/ZnO nanocomposites prepared via nonhydrolytic route*. Journal of Chemical Technology and Metallurgy, 2013. **48**(2): p. 154-161.
16. Yemmireddy, V.K. and Y.C. Hung, *Using Photocatalyst Metal Oxides as Antimicrobial Surface Coatings to Ensure Food Safety-Opportunities and Challenges*. Compr Rev Food Sci Food Saf, 2017. **16**(4): p. 617-631.
17. Patil, M., S. Shaikh, and G. Ibram, *Recent Advances on TiO₂ Thin Film Based Photocatalytic Applications (A Review)*. Current Nanoscience, 2015. **11**.
18. Varshney, G., et al., *Nanoscale TiO₂ films and their application in remediation of organic pollutants*. Coordination Chemistry Reviews, 2016. **306**: p. 43-64.
19. Mardare, D., et al., *Undoped and Cr-doped TiO(2) thin films obtained by spray pyrolysis*. Thin Solid Films, 2010. **518**: p. 4586-4589.
20. Deák, Á., et al., *Layered double oxide (LDO) particle containing photoreactive hybrid layers with tunable superhydrophobic and photocatalytic properties*. Applied Surface Science, 2016. **389**.
21. Mérai, L., et al., *Photoreactive composite coating with composition dependent wetting properties*. Express Polymer Letters, 2018. **12**: p. 1061-1071.
22. Pant, Park, and Park, *Recent Advances in TiO₂ Films Prepared by Sol-gel Methods for Photocatalytic Degradation of Organic Pollutants and Antibacterial Activities*. Coatings, 2019. **9**(10).
23. Jilani, A., M.S. Abdel-wahab, and A.H. Hammad, *Advance Deposition Techniques for Thin Film and Coating*, in *Modern Technologies for Creating the Thin-film Systems and Coatings*. 2017.
24. Aguilar, G., *Introductory Chapter: A Brief Semblance of the Sol-Gel Method in Research*. 2018.
25. C. Brinker, G.S., *The Physics and Chemistry of Sol-Gel Processing*. 1st ed. 1990, Academic Press: Academic Press. 912.
26. Dulian, P., et al., *Photocatalytic methylene blue degradation on multilayer transparent TiO₂ coatings*. Optical Materials, 2019. **90**: p. 264-272.

27. Khlyustova, A., et al., *Doped TiO₂: the effect of doping elements on photocatalytic activity*. Materials Advances, 2020. **1**(5): p. 1193-1201.
28. Norton, D.P., et al., *ZnO: growth, doping & processing*. Materials Today, 2004. **7**(6): p. 34-40.
29. Bensouici, F., et al., *Synthesis, characterization and photocatalytic behavior of Ag doped TiO₂ thin film*. Superlattices and Microstructures, 2015. **85**: p. 255-265.
30. Tan, Y. and D.E. Resasco, *Dispersion of Single-Walled Carbon Nanotubes of Narrow Diameter Distribution*. The Journal of Physical Chemistry B, 2005. **109**(30): p. 14454-14460.
31. Brady, J.B. and S.J. Boardman, *Introducing Mineralogy Students to X-Ray Diffraction through Optical Diffraction Experiments using Lasers*. Journal of Geological Education, 1995. **43**(5): p. 471-476.
32. Valerio, A. and S. Morelhão, *Usage of Scherrer's formula in X-ray diffraction analysis of size distribution in systems of monocrystalline nanoparticles*. 2019.
33. Phuinthiang, P., et al., *Novel Strategy for the Development of Antibacterial TiO₂ Thin Film onto Polymer Substrate at Room Temperature*. Nanomaterials, 2021. **11**(6).
34. Sayılkan, F., et al., *Photocatalytic antibacterial performance of Sn⁴⁺-doped TiO₂ thin films on glass substrate*. Journal of Hazardous Materials, 2009. **162**(2): p. 1309-1316.
35. Pleskova, S.N., et al., *Photoinduced bactericidal activity of TiO₂ films*. Applied Biochemistry and Microbiology, 2011. **47**(1): p. 23-26.
36. Gospodonova, D., I. Ivanova, and T. Vladkova, *Fabrication and Characterization of Antimicrobial Magnetron Cosputtered TiO₂/Ag/Cu Composite Coatings*. Coatings, 2021. **11**(4).
37. Nithya, N., et al., *Evaluation of gas sensor behaviour of Sm³⁺ doped TiO₂ nanoparticles*. Journal of Materials Science: Materials in Electronics, 2021.
38. Natsir, M., et al., *Synthesis and characterization of Cu-doped TiO₂ (Cu/TiO₂) nanoparticle as antifungal phytophthora palmivora*. Journal of Physics: Conference Series, 2021. **1899**(1): p. 012039.
39. Chobba, M.B., et al., *Ag-TiO₂/PDMS nanocomposite protective coatings: Synthesis, characterization, and use as a self-cleaning and antimicrobial agent*. Progress in Organic Coatings, 2021. **158**: p. 106342.

40. Najibi Ilkhechi, N., M. Mozammel, and A. Yari Khosroushahi, *Antifungal effects of ZnO, TiO₂ and ZnO-TiO₂ nanostructures on Aspergillus flavus*. *Pesticide Biochemistry and Physiology*, 2021. **176**: p. 104869.